Laser and Particle Beams (2007), *25*, 71–77. Printed in the USA.
Copyright © 2007 Cambridge University Press 0263-0346/07 $20.00
DOI: 10.1017/S0263034607070115

Laser triggered micro-lens for focusing and energy selection of MeV protons

O. WILLI,[1] T. TONCIAN,[1] M. BORGHESI,[2] J. FUCHS,[3] E. D'HUMIÈRES,[3,4] P. ANTICI,[3] P. AUDEBERT,[3] E. BRAMBRINK,[3] C. CECCHETTI,[2] A. PIPAHL,[1] AND L. ROMAGNANI[2]

[1]Heinrich Heine Universität Düsseldorf, Düsseldorf, Germany
[2]The Queen's University Belfast, Belfast, Northern Ireland, United Kingdom
[3]LULI, Ecole Polytechnique, Palaiseau, France
[4]Centre de Physique Théorique, CNRS-Ecole Polytechnique, Palaiseau, France

(RECEIVED 22 September 2006; ACCEPTED 18 October 2006)

Abstract

We present a novel technique for focusing and energy selection of high-current, MeV proton/ion beams. This method employs a hollow micro-cylinder that is irradiated at the outer wall by a high intensity, ultra-short laser pulse. The relativistic electrons produced are injected through the cylinder's wall, spread evenly on the inner wall surface of the cylinder, and initiate a hot plasma expansion. A transient radial electric field (10^7–10^{10} V/m) is associated with the expansion. The transient electrostatic field induces the focusing and the selection of a narrow band component out of the broadband poly-energetic energy spectrum of the protons generated from a separate laser irradiated thin foil target that are directed axially through the cylinder. The energy selection is tunable by changing the timing of the two laser pulses. Computer simulations carried out for similar parameters as used in the experiments explain the working of the micro-lens.

Keywords: Laser triggered ion micro-lens; Proton focusing; Quasi mono-energetic proton beam

1. INTRODUCTION

During the interaction of ultra-intense laser pulses with thin solid foil targets ($I > 10^{19}$ W/cm^2), a considerable fraction of the laser energy is deposited into highly energetic ions. In particular, a collimated beam of protons with energies up to tens of MeV is ejected from the rear side perpendicular to the surface of the target (Clark *et al*., 2000; Snavely *et al*., 2000). The protons originate from hydro-carbon impurities located on the surfaces of the target, so that proton beams are observed even when using targets which nominally do not contain hydrogen. The protons are accelerated via target normal sheath acceleration (TNSA) mechanism (Wilks *et al*., 2001; Mora, 2003; Romagnani *et al*., 2005) and via a recently proposed laser break-out afterburner (BOA) process (Yin *et al*., 2006). The characteristics of the proton beam are of small source size, low divergence, short duration, and has a large density (Borghesi *et al*., 2004, 2005). These laser produced proton beams have opened up new opportunities for major applications in scientific, technological, and medical areas. The proposed applications include energy production via thermonuclear fusion (Roth *et al*., 2001), cancer therapy (Bulanov *et al*., 2002), production of radioactive particles for medical diagnosis (Spencer *et al*., 2001), and the detection of electric and magnetic fields in plasmas (Borghesi *et al*., 2002, 2003; Mackinnon *et al*., 2004; Romagnani *et al*., 2005). However, reduction and control of the angular divergence and of the energy spread of these pulses are essential requirements for some of these applications. So far, mainly target engineering techniques have been employed to overcome these short-comings. For example, geometrical focusing of laser-driven protons has been attained by using curved targets (Patel *et al*., 2003). However, this technique has been limited so far to focal distances of a few mm, and to the low energy component of the proton spectrum. In addition, recently a quasi-monochromatic acceleration from laser irradiated micro-structured targets has been reported (Hegelich *et al*., 2006; Schwoerer *et al*., 2006). In these approaches, the focusing or energy selection effect is achieved by directly acting on the source. As a consequence, these techniques rely on relatively complex target fabrication and preparation procedures. An alternative approach that provides a tunable, simultaneous focus-

Address correspondence and reprint requests to: Oswald Willi, Institut für Laser- und Plasmaphysik, Universitätsstr. 1, Geb. 25.33, D-40225 Düsseldorf. Germany. E-mail: oswald.willi@laserphy.uni-duesseldorf.de

https://doi.org/10.1017/S0263034607070115 Published online by Cambridge University Press

ing and an energy selection of MeV proton beams has recently been proposed and demonstrated (Toncian *et al*., 2006; Willi *et al*., 2005). An analytical scaling law for the laser driven micro-lens has recently been derived by Gordienko *et al*. (2006). The new approach decouples the beam tailoring stage from the acceleration stage allowing for their independent optimization. The technique employs electric fields generated for a very short time within a micro-cylinder irradiated by a short, intense laser pulse. These fields can focus efficiently a proton beam directed along the axis of the cylinder. An important point is that only protons reaching the cylinder while the fields are active (i.e., only protons with a specific velocity) will be focused. By spatial filtering out the unfocused part of the beam, it is therefore possible to select only protons that have the same velocity producing a narrow band energy spectrum. This paper describes some characteristics of the laser-triggered micro-lens.

2. EXPERIMENTAL ARRANGEMENT

The experiment was carried out at the Laboratory for the Use of Intense Lasers (LULI), employing the 100 TW laser (Wattellier *et al*., 2004) operating in the chirped pulse amplification mode (CPA). After amplification, the laser pulse was split into two separate pulses that were then recompressed in separate grating compressors. This allowed the use of two pulses (CPA_1 and CPA_2) of 350 fs and 350 fs for 1.2 ps duration. The short pulses are preceded by an amplified spontaneous emission (ASE) pedestal starting a few ns before the high intensity peak. The main-to-prepulse contrast ratio was better than 10^7 at 20 ps before the main-pulse. The delay between the two CPA pulses was controlled optically with picosecond precision. The CPA_1 pulse was focused with an $f/3$ off axis parabola (OAP) onto a 10 μm thick Au foil target resulting in an intensity of 3×10^{19} W/cm^2 and accelerating a high-current, diverging beam of up to 15 MeV protons. The CPA_2 pulse was focused by a similar parabola onto a hollow cylinder to an intensity of 3×10^{18} W/cm^2. The proton beam from the first foil was directed through the cylinder and detected with a stack of gafchromic radiochromic films (RCF) (a dosimetric detector) positioned at a variable (from 2 to 70 cm) distance from the proton source (see Fig. 1).

Generally, the cylinder made of dural was 3 mm in length, 700 μm in diameter, and 50 μm in wall thickness. The distance between the proton production foil and cylinder and the distance between the cylinder and detector were varied throughout the experiment. At a source-cylinder distance of 1 mm, the proton flux increase due to focusing by the micro-lens was so strong that saturation of the film occurred. Quantitative data could only be obtained when the cylinder was moved to 4 mm from the proton foil, in order to collect a smaller part of the diverging proton beam. In this case, the distance from the proton-producing foil to the CPA_2 irradiation point on the cylinder was 5 mm (standard experimental configuration). The RCF stack was used to measure the proton beam divergence. It was shielded with an 11 μm Al foil allowing protons with energies above 1.5 MeV to be recorded. It also provided a coarse energy resolution due to the energy deposition properties of the ions (most of the energy of a proton is released in the so-called Bragg peak, located at a distance in the detector which depends on the incident proton energy). In some cases, a central mm-sized hole was cut through the RCF to allow downstream high spectral resolution measurements using a magnetic spectrometer with a 0.6 T permanent magnet. The spectral resolution determined by the slit width and the dispersion of the spectrometer is 0.2 MeV at 6 MeV and 0.7 MeV at 15 MeV.

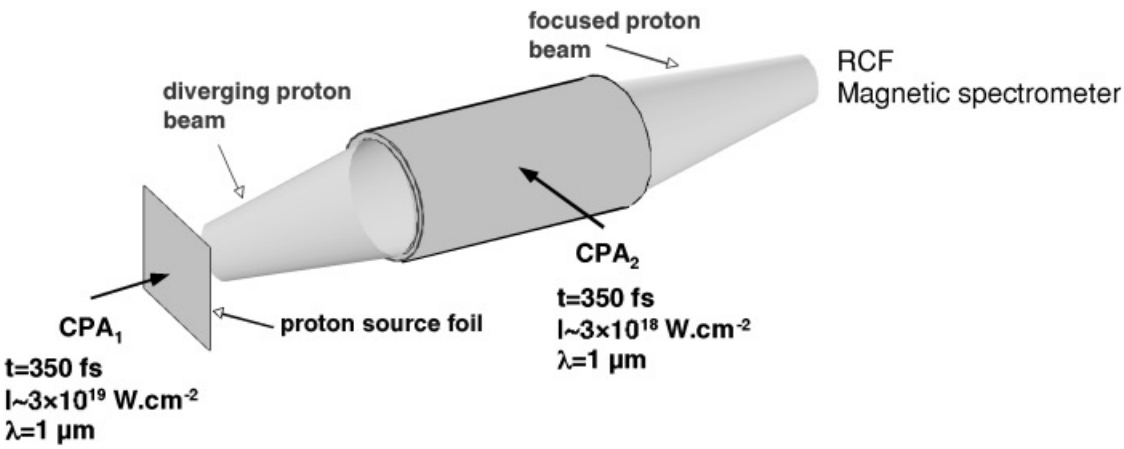

Fig. 1. Schematic of the micro-lens device. A proton beam accelerated from a planar foil by the CPA_1 laser pulse propagates through a hollow cylinder side-irradiated by the CPA_2 pulse.

https://doi.org/10.1017/S0263034607070115 Published online by Cambridge University Press

3. EXPERIMENTAL RESULTS

Figure 2A shows different layers (the 5th and 6th in the stack, corresponding to protons of 9 and 7.5 MeV, respectively) of an RCF pack recording the proton beam after its propagation through a laser-illuminated dural cylinder in the standard experimental configuration. As expected, no focusing effect is observed for the 9 MeV protons. Indeed, the electric field is triggered by the CPA_2 laser pulse ~20 ps after these protons exit the cylinder. For the 7.5 MeV protons, the electric field just develops while these protons are close to exit the cylinder and a small spot about 600 μm (FWHM) in diameter is seen on the RCF at the center of the cylinder's shadow. In this case, the proton flux within the spot at the film plane is increased by up to 12 times compared to the unfocused part not captured by the cylinder (Fig. 2B). Focal spots as small as 200 μm have been observed depending on the detector position. In this case, the proton flux within the spot at the film plane is increased by up to 15 times compared to the unfocused part not captured by the cylinder.

In Figure 3, the spot sizes for the different energies are shown for a 0.9 diameter cylinder, 1 mm in length, and placed 1 mm from the rear side of the proton producing foil target. As the film was saturated with the energies between 6 and 8 MeV, the plotted spot size gives an upper limit.

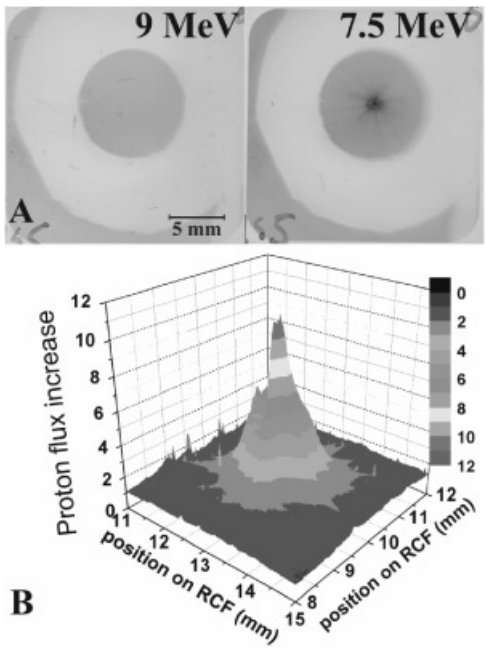

Fig. 2. (**A**) RCF layers showing the proton beam focusing effect due to a 3 mm long, 700 μm diameter dural (95% Al, 4% Cu and 1% Mg) lasers irradiated cylinder with 50 μm wall thickness. For the energies reaching the Bragg peak in the two layers shown, the protons with an energy of 9 MeV pass through the cylinder before the electric field is present showing no focusing whereas the divergence of the protons with an energy of 7.5 MeV is strongly reduced by the electric field that has developed inside the cylinder. The shadow of the cylinder and of the 50 μm W holding wire can clearly be seen. (**B**) Flux increase with respect to the unfocused flux for 7.5 MeV protons as deduced from the layer shown in (A).

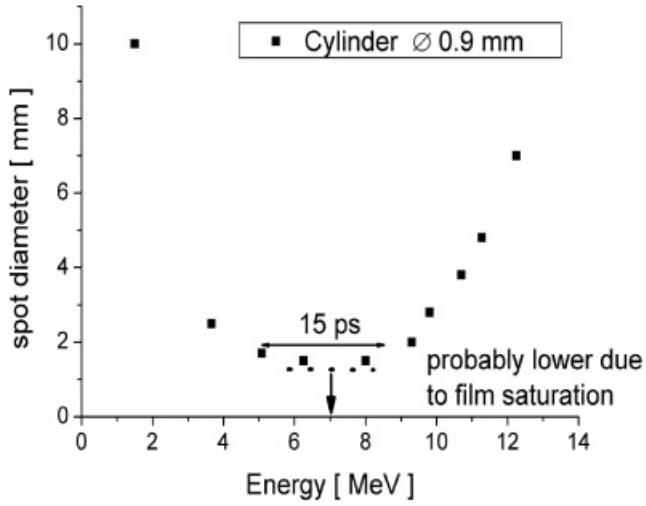

Fig. 3. The energy dependence of proton beam FWHM spot size measured in the detector plane for another shot where the proton source-cylinder distance was 1 mm and the cylinder diameter was 0.9 mm.

In addition, we have studied the evolution of the beam size, as a function of the propagation distance from the cylinder. The behavior of the 7.5 MeV proton components is illustrated in Figure 4. Note that for this energy, the beam size is only 8 mm after 70 cm of propagation whereas freely propagating; the size of the beam would have been 260 mm.

Figure 5 shows the spectrum obtained, again for the same standard experimental configuration, using the magnetic spectrometer, with an entrance slit of 250 μm positioned 70 cm away from the proton source. As a reference, we also show a typical exponential spectrum collected in the same conditions, but without the micro-lens. The data shows

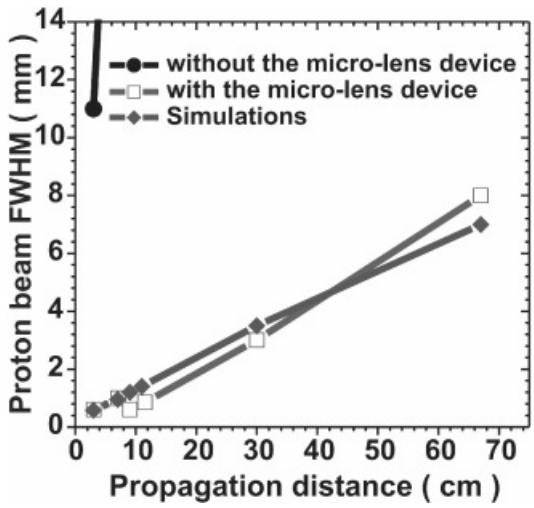

Fig. 4. Evolution of the FWHM of the proton beam, for protons with energy of 7.5 MeV. The circles correspond to the case without micro-lens (free-space divergence), the diamonds to the particle-tracer simulation in the fields given by the PIC simulation, and the squares to the experimental results using the micro-lens.

https://doi.org/10.1017/S0263034607070115 Published online by Cambridge University Press

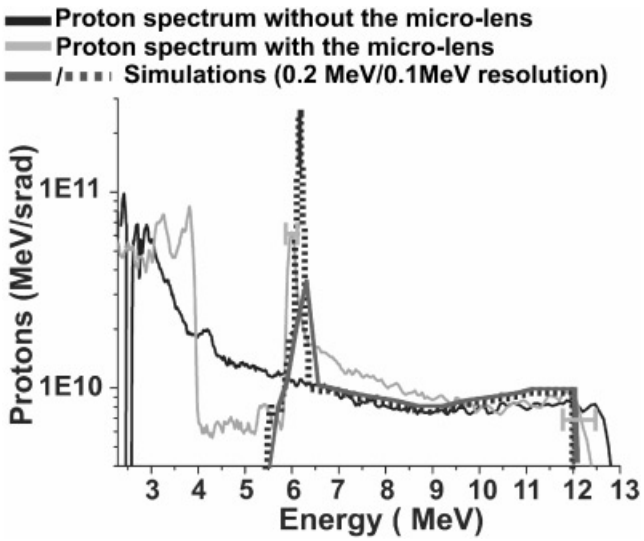

Fig. 5. Experimental proton spectra without micro-lens (solid line) and with the micro-lens (dashed line) and the simulated proton spectrum (dotted lines). The simulated spectrum was obtained by tracing 5000 protons through the fields predicted by the simulations.

clearly the energy selection capability of the micro-lens: due to selective collimation of the 6.25 MeV protons, these could be transmitted efficiently through the spectrometer slit (acting as an angular filter), and their density after the slit in the spectrally dispersed plane is enhanced as compared to the free-space expansion case. For this shot, the 6.25 MeV protons experience the focusing fields for ~5 ps before exiting the cylinder. Note that an energy spread of 0.2 MeV was obtained. Hence for the energy peak around 6 MeV, a $\Delta E/E$ of ~ 3% was achieved. The energy spread was, however, limited by the resolution of the spectrometer.

As shown in Figure 5, the simulations performed for the same conditions as in the experiment, suggest that the spectral width of the peak is around 0.1 MeV and hence narrower than demonstrated by the experimental spectrum shown. By varying the optical delay between the laser beams, the location of this peak on the energy axis can be tuned selectively, therefore allowing tailoring the energy distribution of the transmitted beam, a necessary step for many of the applications mentioned earlier. We would like to emphasize that with this approach focusing and energy selection are provided simultaneously.

In order to investigate the underlying physics of the micro-lens, a cylinder with a gap along the axis with a width of about 100 μm was irradiated. With the gap in the cylinder, the focusing characteristics were changed. The focused proton spot is not symmetric anymore and shows caustics in the direction to the slit as shown in Figure 6. This data indicates that electric fields are responsible for the focusing of the protons. To ensure that focusing is not produced by electric fields at the ends of the cylinder, the ends were closed using 3 μm Al foils. In this case, no difference as with open cylinders was seen in the focusing. A clear difference however was seen when plastic cylinders were used. The spots were larger and less uniform. In addition, the diameter of the target support stalk changed the lens characteristics. The divergence of the proton beam was significantly smaller for 50 μm wires than for 500 μm wires.

4. SIMULATIONS

For better understanding of the micro-lens one-dimensional (1D) simulations of field generation at the micro-lens' walls and three-dimensional (3D) test-particle simulations of proton propagation through the micro-lens were performed.

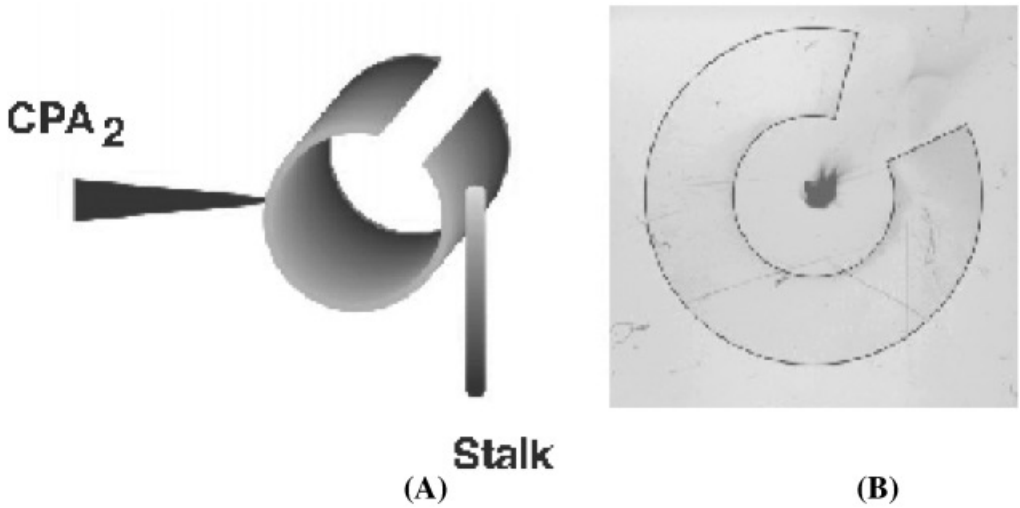

Fig. 6. Laser irradiated cylinder with a slit along the axial direction shows that the focus of the proton beam is degraded. (**A**) shows the schematic of the target and laser arrangement and the RCF illustrating the focus of the proton beam together with the outline of the initial cylinder are shown in (**B**).

https://doi.org/10.1017/S0263034607070115 Published online by Cambridge University Press

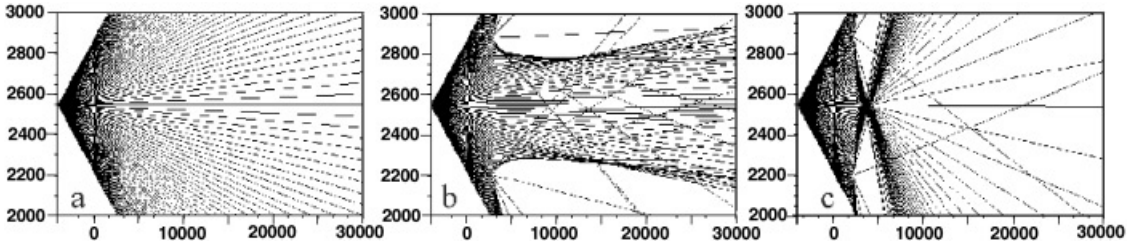

Fig. 7. (**a**) Trajectories for 7.6 MeV, (**b**) 6.25 MeV, and (**c**) 4.9 MeV. Note that the two axes (in units of microns) in all three simulations are not scaled in the same way. This is for clarity.

The protons passing along the axis of the cylinder can either be focused by a radial electric or azimuthally magnetic field. The simulations were performed in two steps using the CALDER code (Lefebvre *et al*., 2003). We used 1D simulation, corresponding to the transverse direction to the cylinder's axis to simulate directly the plasma expansion from a 700 μm diameter cylinder. The cylinder, which has a thickness of 50 μm, is irradiated by a laser pulse at an intensity 3×10^{18} W/cm^2, and with a pulse duration of 350 fs. Finally we propagate protons in the cylinder through the space and time dependent simulated fields, using a proton beam with the experimental divergence, energy spectrum, and experimental time delay. The initial temperature of the hot electrons considered in the PIC simulation is 400 keV, as given by the lasers ponder motive potential in the laser field at the irradiance used. The initial electron density at the cylinder's wall is estimated by considering that a 40% (inferred from experimental measurements) fraction of the laser energy is converted into hot electron, and then that these are spread evenly on the cylinder's walls. This results in a hot electron density of $\sim 6 \times 10^{16}$ cm^{-3}. We assume that when the plasma expansion starts, the field obtained by the PIC simulation is the same for the total length of the cylinder, e.g., for all $x \in [0, 3000\ \mu\text{m}]$. As in the experiment, the protons are produced at $x = -4000\ \mu$m and $y = 2547\ \mu$m, and they propagate through the cylinder. Figure 7 shows simulated trajectories for 100 protons at 7.6, 6.25, and 4.9 MeV. The 7.6 MeV protons exit the cylinder before it is triggered (Fig. 7a). These protons retain their initial large divergence. The 6.25 MeV protons are in the cylinder when it is triggered, although close to its end. These protons are clearly collimated as seen in Figure 7b and therefore create a strong peak at the plane of the RCF (3.5 cm from the source). The protons 4.9 MeV (Fig. 7c) is closer to the middle of the cylinder when it is triggered, so they see a stronger field than the 6 MeV protons along their path in the cylinder. As a consequence, these protons are actually focused tightly at a very short distance from the micro-lens exit plane and diverge also strongly after this focusing point.

5. DISCUSSION

The computational results support the scenario in which laser-triggered transient fields drive the selective deflection of the protons. The physical mechanisms behind the micro-lens operation are as follows: when the laser pulse irradiates the outer side of the cylinder, it produces a population of hot electrons which penetrate through the wall and spread very quickly over the inner surface of the cylinder. They then exit into a vacuum resulting in an electron cloud in the surface surrounding area. The associated space-charge field is large enough to ionize the material at the cylinder surface and to create plasma. This results in a cylindrical plasma layer with high electron temperature. The plasma begins to expand toward the cylinder axis, driven by a hot electron sheath that extends over a Debye length ahead of the plasma as shown in Figures 8A and 8B.

The radically symmetric ambipolar electrostatic field associated with the plasma front is responsible for the variable focusing of the protons propagating along the cylinder's axis. The poly-energetic protons arrive in the cylinder at different times due to their different velocities, with higher energy protons crossing the cylinder at earlier times. Protons passing through the micro-lens before it is triggered do not experience any fields and are therefore not deflected. Protons that are crossing the cylinder and are close to its end when it is triggered and therefore experience the fields for only a short time will be collimated. Lower energy protons will experience a larger cumulated field along their propagation through the cylinder. They are therefore focused at a short distance from the exit plane of the micro-lens and diverge strongly after focus. These results in a diluted beam

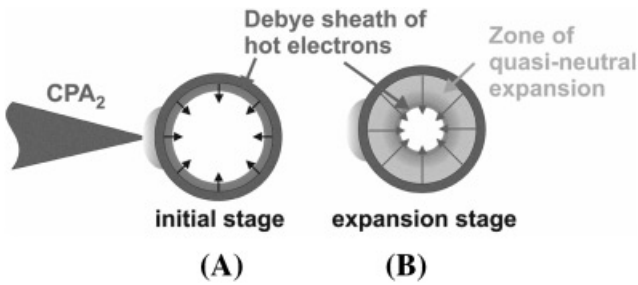

Fig. 8. Schematic of the operation's principle of the micro-lens. The CPA_2 laser pulse injects hot electrons through the wall of the cylinder. They spread very quickly over the inner surface of the cylinder. (**A**) shows that the associated space-charge field is large enough to ionize the material at the cylinder surface and to create plasma. These electrons generate a space-charge field (indicated by the radically pointing arrows), which then induces a plasma expansion from the cylinder's inner walls shown in (**B**).

https://doi.org/10.1017/S0263034607070115 Published online by Cambridge University Press

on the RCF stack positioned a few cm away and in the strong dip observed in the spectrum of Figure 5 below 6 MeV.

The micro-lens is easily tunable through the energy spectrum. This is because the different energy components of the ion beam separated by time-of-flight dispersion, transit through the micro-lens at different times, and are affected differently by the transient electric fields present in the lens. Some energy components are focused, some are only collimated, and the focusing distance is energy-dependent, allowing for energy selection by spatial filtering of the focused component. Intrinsic tune ability is provided by simply laser-triggering the micro-lens at different times.

6. CONCLUSIONS

We have presented a novel technique for focusing and energy selection of high-current MeV proton/ion beams. The laser driven hollow micro-lens represents a major step in making the laser-accelerated ion sources more attractive for various applications. While retaining the exceptional beam quality of laser-accelerated ion sources, the micro-lens provides a solution to two of the main obstacles still preventing widespread applicability of these sources, namely their broad divergence and their large energy spread. The device applies to laser-driven protons as well as any ion beam. This method does not involve complex target engineering and alignment procedures and decouples the focusing and energy selection steps from the generation of the proton or ion source. In addition, the focusing effect can be scaled up to very high ion energies as discussed by Toncian *et al*. (2006).

ACKNOWLEDGMENTS

We acknowledge fruitful discussions with L. Gremillet, T. Grismayer, S. Gordienko, E. Lefebvre, P. Mora and A. Pukhov. We thank Erik Lefebvre for allowing us to use his PIC code CALDER, and the CEA/DAM for the simulations we performed on the CCRT computers. We acknowledge the expert support from the technical teams at LULI. This work has been supported by EU-Grant No. HPRICT 1999-0052, Grant No. E1127 from Région Ile-de-France, and DFG TR18 and GK1203, and partly by the QUB-IRCEP scheme and DAAD.

REFERENCES

Borghesi, M., Audebert, P., Bulanov, S.V., Cowan, T., Fuchs, J., Gauthier, J.C., MacKinnon, A.J., Patel, P.K., Pretzler, G., Romagnani, L., Schiavi, A., Toncian, T. & Willi, O. (2005). High-intensity laser-plasma interaction studies employing laser-driven proton probes. *Laser Part. Beams* **23**, 291–295.

Borghesi, M., Bulanov, S., Campbell, D.H., Clarke, R.J., Esirkepov, T.Z., Galimberti, M., Gizzi, L.A., MacKinnon, A.J., Naumova, N.M., Pegoraro, F., Ruhl, H., Schiavi, A. & Willi, O. (2002). Macroscopic evidence of soliton formation in multiterawatt laser-plasma interaction. *Phys. Rev. Lett.* **88**, 135002/1-4.

Borghesi, M., MacKinnon, A.J., Campbell, D.H., Hicks, D.G., Kar, S., Patel, P.K., Price, D., Romagnani, L., Schiavi, A. & Willi, O. (2004). Multi-MeV proton source investigations in ultra intense laser-foil interactions. *Phys. Rev. Lett.* **92**, 055003/1–4.

Borghesi, M., Schiavi, A., Campbell, D.H., Haines, M.G., Willi, O., MacKinnon, A.J., Patel, P., Galimberti, M. & Gizzi, L.A. (2003). Proton imaging detection of transient electromagnetic fields in laser-plasma interactions (invited). *Revi. Sci. Instr.* **74**, 1688–1693.

Bulanov, S.V., Esirkepov, T.Z., Khoroshkov, V.S., Kunetsov, A.V. & Pegoraro, F. (2002). Oncological hydrotherapy with laser ion accelerators. *Phys. Lett. A* **299**, 240–247.

Clark, E.L., Krushelnick, K., Davies, J.R., Zepf, M., Tatarakis, M., Beg, F.N., Machacek, A., Norreys, P.A., Santala, M.I.K., Watts, I. & Dangor, A.E. (2000). Measurements of energetic proton transport through magnetized plasma from intense laser interactions with solids. *Phys. Rev. Lett.* **84**, 670–673.

Gordienko, S., Baeva, T. & Pukhov, A. (2006). Focusing of laser-generated ion beams by a plasma cylinder: Similarity theory and the thick lens formula. *Phys. Plasmas* **13**, 063103/1–6.

Hegelich, B.M., Albright, B.J., Cobble, J., Flippo, K., Letzring, S., Paffett, M., Ruhl, H., Schreiber, J., Schulze, R.K. & Fernandez, J.C. (2006). Laser acceleration of quasi-monoenergetic MeV ion beams. *Nature* **439**, 441–444.

Lefebvre, E., Cochet, N., Fritzler, S., Malka, V., Aleonard, M.M., Chemin, J.F., Darbon, S., Disdier, L., Faure, J., Fedotoff, A., Landoas, O., Malka, G., Meot, V., Morel, P., Le Gloahec, M.R., Rouyer, A., Rubbelynck, C., Tikhonchuk, V., Wrobel, R., Andebert, P. & Rousseaux, C. (2003). Electron and photon production from relativistic laser-plasma interactions. *Nucl. Fusion* **43**, 629–633.

MacKinnon, A.J., Patel, P.K., Town, R.P., Edwards, M.J., Phillips, T., Lerner, S.C., Price, D.W., Hicks, D., Key, M.H., Hatchett, S., Wilks, S.C., Borghesi, M., Romagnani, L., Kar, S., Toncian, T., Pretzler, G., Willi, O., Koenig, M., Martinolli, E., Lepape, S., Benuzzi-Mounaix, A., Audebert, P., Gauthier, J.C., King, J., Snavely, R., Freeman, R.R. & Boehlly, T. (2004). Proton radiography as an electromagnetic field and density perturbation diagnostic. *Rev. Sci. Instr.* **75**, 3531–3536.

Mora, P. (2003). Plasma expansion into a vacuum. *Phys. Rev. Lett.* **90**, 185002/1-4.

Patel, P.K., MacKinnon, A.J., Key, M.H., Cowan, T.E., Foord, M.E., Allen, M., Price, D.F., Ruhl, H., Springer, P.T. & Stephens, R. (2003). Isochoric heating of solid-density matter with an ultrafast proton beam. *Phys. Rev. Lett.* **91**, 125004/1–4.

Romagnani, L., Fuchs, J., Borghesi, M., Antici, P., Audebert, P., Ceccherini, F., Cowan, T., Grismayer, T., Kar, S., Macchi, A., Mora, P., Pretzler, G., Schiavi, A., Toncian, T. & Willi, O. (2005). Dynamics of electric fields driving the laser acceleration of multi-MeV protons. *Phys. Rev. Lett.* **95**, 195001/1–4.

Roth, M., Cowan, T.E., Key, M.H., Hatchett, S.P., Brown, C., Fountain, W., Johnson, J., Pennington, D.M., Snavely, R.A., Wilks, S.C., Yasuike, K., Ruhl, H., Pegoraro, F., Bulanov, S.V., Campbell, E.M., Perry, M.D. & Powell, H. (2001). Fast ignition by intense laser-accelerated proton beams. *Phys. Rev. Lett.* **86**, 436–439.

Schwoerer, H., Pfotenhauer, S., Jackel, O., Amthor, K.U., Liesfeld, B., Ziegler, W., Sauerbrey, R., Ledingham,

https://doi.org/10.1017/S0263034607070115 Published online by Cambridge University Press

K.W.D. & Esirkepov, T. (2006). Laser-plasma acceleration of quasi-monoenergetic protons from microstructured targets. *Nature* **439**, 445–448.

Snavely, R.A., Key, M.H., Hatchett, S.P., Cowan, T.E., Roth, M., Phillips, T.W., Stoyer, M.A., Henry, E.A., Sangster, T.C., Singh, M.S., Wilks, S.C., MacKinnon, A., Offenberger, A., Pennington, D.M., Yasuike, K., Langdon, A.B., Lasinski, B.F., Johnson, J., Perry, M.D. & Campbell, E.M. (2000). Intense high-energy proton beams from petawatt-laser irradiation of solids. *Phys. Rev. Lett.* **85**, 2945–2948.

Spencer, I., Ledingham, K.W.D., Singhal, R.P., McCanny, T., McKenna, P., Clark, E.L., Krushelnick, K., Zepf, M., Beg, F.N., Tatarakis, M., Dangor, A.E., Norreys, P.A., Clarke, R.J., Allott, R.M. & Ross, I.N. (2001). Laser generation of proton beams for the production of short-lived positron emitting radioisotopes. *Nucl. Inst. Meth. Phys. Res. B* **183**, 449–458.

Toncian, T., Borghesi, M., Fuchs, J., d'Humieres, E., Antici, P., Audebert, P., Brambrink, E., Cecchetti, C.A., Pipahl, A., Romagnani, L. & Willi, O. (2006). Ultrafast laser-driven micro lens to focus and energy-select mega-electron volt protons. *Science* **312**, 410–413.

Wattellier, B., Fuchs, J., Zou, J.P., Abdeli, K., Pepin, H. & Haefner, C. (2004). Repetition rate increase and diffraction-limited focal spots for a nonthermal-equilibrium 100-TW Nd : glass laser chain by use of adaptive optics. *Opt. Lett.* **29**, 2494–2496.

Wilks, S.C., Langdon, A.B., Cowan, T.E., Roth, M., Singh, M., Hatchett, S., Key, M.H., Pennington, D., MacKinnon, A. & Snavely, R.A. (2001). Energetic proton generation in ultra-intense laser–solid interactions. *Phys. Plasmas* **8**, 542–549.

Willi, O., Toncian, T., Borghesi, M. & Fuchs, J. (2005). Laserbestrahlter Hohlzylinder als Linse für Ionenstrahlen. *Deutsche Patentanmeldung* 10 2005 012 059.8 PILZ.

Yin, L., Albright, B.J, Hegelich, B.M. & Fernandez, J.C. (2006). GeV laser ion acceleration from ultrathin targets: The laser break-out afterburner. *Laser Part. Beams* **24**, 291–298.

https://doi.org/10.1017/S0263034607070115 Published online by Cambridge University Press